A NEW EXPERIMENTAL TEST RIG FOR PERFORMANCE ANALYSIS OF RADIAL COMPRESSORS INSIDE INNOVATIVE HEAT PUMPS

Marco Ferrando [1]
Università degli Studi di Genova, TPG, Genova, Italy

Tommaso Reboli
Università degli Studi di Genova, TPG, Genova, Italy

Sreenath Purushothaman
Università degli Studi di Genova, TPG, Genova, Italy

Alberto Traverso
Università degli Studi di Genova, TPG, Genova, Italy

Chaitanya Halbe
Carrier Corporation, East Syracuse, USA

ABSTRACT

Electrification is playing a major role in the industrial and energy sector, with heat pump (HP) market expected to grow significantly in the next future in accordance with the current energy transition phase, which aims to reduce the utilization of fossil fuels for heat production sector. It is therefore of crucial importance to find new ways to increase heat pump performance and reliability, containing maintenance costs. The use of dynamic compressors in HPs makes it possible to combine good performance with high compactness and silent operation, but unlike the volumetric compressor, this equipment could undergo dangerous instability during operation, which can occur in closed-cycle configuration, quite unusual for dynamic compressors. The aim of this paper is to present a new test-rig for stable and unstable performance analysis of dynamic compressors for innovative heat pumps. An in-depth description of the plant and instrumentation system is provided. The performance of the compressor is analyzed for different operating points, with a particular focus on near-surge operation. Experimental uncertainties and their reduction through data reconciliation techniques is thoroughly investigated.

NOMENCLATURE

Symbols

h	Enthalpy	[J/kg]
$\dot{m}$	Mass flow	[kg/s]
n	Rotational speed	[rpm]
P	Pressure	[bar]
T	Temperature	[K]
$\dot{V}$	Volumetric flow	[m3/s]

Greek letters

β	Pressure ratio	[-]
σ	Standard deviation	[-]

Subscripts

C	Condenser
E	Evaporator
R	Refrigerant
Red	Reduced
Ref	Reference
T	Total
W	Water
1	Inlet
2	Outlet

Acronyms & Abbreviations

DAQ	Data Acquisition System
DR	Data Reconciliation
FT	Flow Transducer
HTF	Heat Transfer Fluid
PT	Pressure Transducer
RTD	Resistance Temperature Detector
TC	Thermocouple

1. INTRODUCTION

In the past two decades, advanced research into the field of heat pump (HP) has made it a practical solution to the threat of rising fuel prices and global warming in the heating & cooling of domestic/commercial buildings, as well as in process industries. In the European Union, the residential sector represents 25.4% of final energy use and 20% greenhouse gas emissions [1], [2]. Recovery of waste heat and reduction in greenhouse gas emissions are some of the attractive features of heat pumps over conventional heating/cooling techniques [3], [4]. Commercial heat pumps

---

employing external mechanical work and operating on vapor compression cycles are widely employed nowadays, and some innovative technologies, such as turbines and ejectors replacing the throttling valve, are gaining importance[5] [6]. Amongst these, turbo heat pumps which utilizes radial compressors are preferred, when possible, as they offer compact and silent operation as compared to positive displacement devices.

Turbo heat pumps, which use dynamic compressors, move heat from a low temperature reservoir to a high temperature reservoir, by circulating the refrigerant through a centrifugal compressor, an expansion valve and two heat exchangers – a condenser and an evaporator [7]. The compressor in this system is susceptible to surge & stall instabilities just like any other radial compressors. But the phenomenon of the surge and stall mechanism are more complex than that of an ordinary compressor [8], [9], [10] due to reasons such as the closed-loop system, presence of 2 plenums (evaporator upstream and condenser downstream), the real gas effects and two-phase nature of the refrigerant in the cycle, and, finally, the heat transfer between refrigerant and external water circuit [11]. Hence, the classical compressor dynamic models developed by Greitzer and Moore [12], [13] for open loop systems and later modified by Botha et. al [14] to a closed loop system are not suitable for this kind of application. Song et. al [7] and Kim and Song [11] later developed a model to better match the operation of a radial compressor in a closed loop refrigerant cycle. These developments demonstrate the need for a clear understanding of the operation & performance analysis of a dynamic compressor–driven heat pump.

The test rig presented in this paper is the result of a collaboration between the University of Genoa and Carrier Corporation, the objective of which is to analyze the performance of dynamic compressors in stable conditions and in surge conditions within innovative heat pump cycles. The stable and near-surge operation regimes and alternate methods for condition monitoring are explored in this paper, along with a detailed description of the compressor test rig and operating procedure.

2. METHODOLOGY

To evaluate the performance of the chiller a proper hydraulic circuit was designed, and a proper set of sensors was chosen. In particular, different types of sensors were installed, to evaluate the influence of the measurement chain on the performance of the DAQ.

2.1 Test rig description

The chiller is integrated into a dedicated hydraulic circuit designed to allow different operative conditions, and to control and monitor all main thermodynamic parameters of the machine. Figure 1 shows the simplified P&I diagram of the experimental test rig. In this figure the Heat Transfer Fluid (HTF) lines are indicated by blue while the refrigerant lines are in green.

In accordance with the P&I diagram, Table 1 shows the list of the sensors installed, with a brief description of each type along with their nominal accuracy.
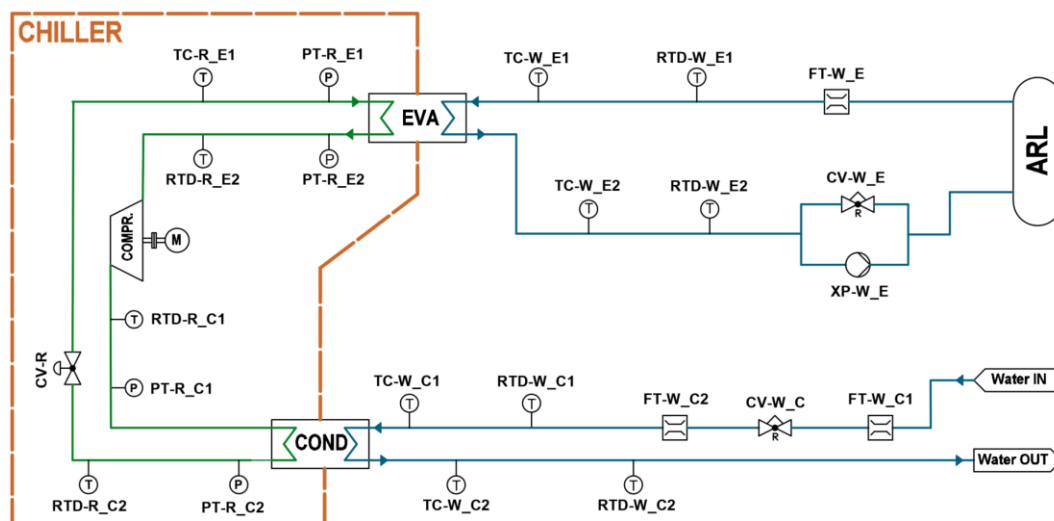

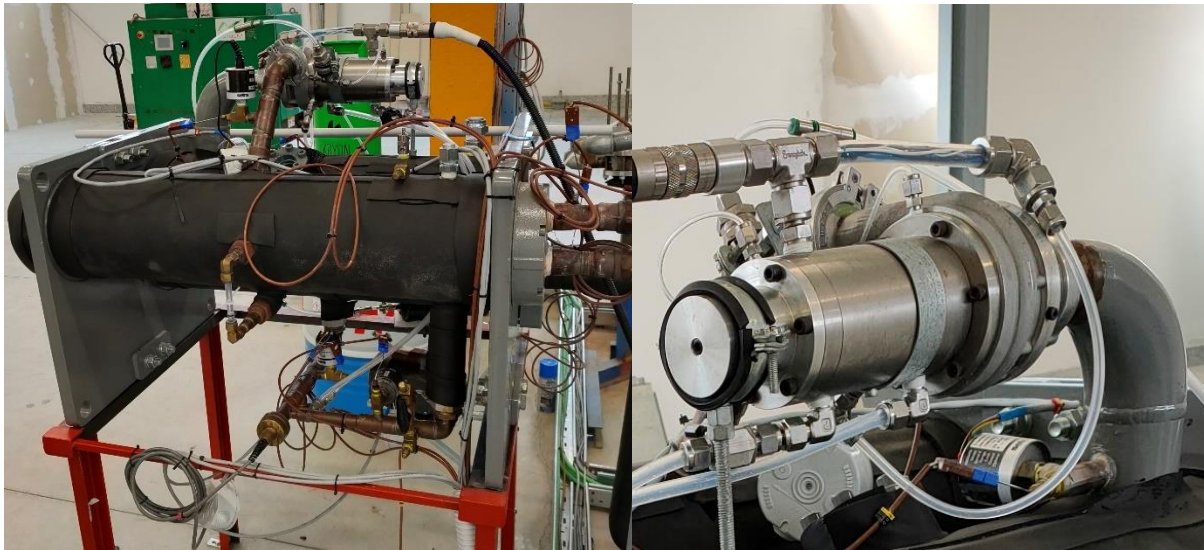Figure 1 – Experimental test rig P&I diagram

Figure 2 – Experimental test rig: overall view of the chiller (left) and detail of the compressor(right)

TAG	Equipment	Manufacturer and model	Accuracy
PT	Pressure transducer (abs)	Setra – Pressure Transmitter 206 [15]	6.9 mbar (0.2% F.s)
TC	Thermocouple	Type T	0.9 K
RTD	Resistance Temperature Detector	Trafag – DIN 1/10 [16]	0.18 K
FT	Flow Transducer	FIP – F3.00 Paddlewheel sensor [17]	See Par. 2.2

Table 1 – Instruments and accuracy

Table 2 shows fluid, thermodynamic properties of the chiller, and maximum compressor performance predicted at the design stage. The fluid used in this chiller is R1233zd-(E) [18]. It is a modern fluid with low Global Warming Potential and used in low pressure applications. As visible, under design conditions at the evaporator the pressure is sub atmospheric.

	Value	Unit
Fluid	R1233zd-(E) [18]	-
Max Compressor speed	75	kRpm
Max electric power	7.5	kW
Max pressure ratio	3.45	-
Evaporator pressure	0.6	bar(a)
Condenser pressure	2.07	bar(a)
Saturation temperature at the evaporator	5.1	°C
Saturation temperature at the condenser	38.7	°C

Table 2 – Design conditions of the chiller

The experimental setup allows varying the operating conditions of the heat pump, and thereby the compressor pressure ratio with great flexibility. The HTF temperatures and flow rates at both the condenser and evaporator sides can be controlled in this test rig, allowing us to evaluate the performance at different operational conditions.

From Figure 1 it can be observed that on some lines multiple sensors are installed, and this allows us to apply data-reconciliation techniques for uncertainty reduction. Specifically, on the "Water IN" branch, there are two mass flow sensors installed in series (FT-W_C1 and FT-W_C2). Moreover, in each branch connected to the evaporator and the condenser (on water side) there are a series of thermal probes installed. For example, at the evaporator inlet there is a series of a RTD (RTD-W_E1) and a thermocouple (TC-W_E1). The choice of using two different sensors is due to the different dynamic response of the two components. The RTDs are more accurate but they have a diameter of 3mm, so they have very slow dynamics. The TCs have lower accuracy but they have a diameter of 1mm, so they detect thermal transients with greater speed. This characteristic of TCs is very important in surge conditions.

2.2 Mass flow sensors calibration and data reconciliation techniques

The FT-W_C1 and FT-W_C2 sensors measure the volumetric flow rate of cooling water to the condenser. These sensors were calibrated together, using an Endress+Hauser Proline Prosonic Flow 91W Ultrasonic flowmeter [19] as the calibrator. The error curve for the calibrator was provided by the manufacturer. Calibration was carried out by keeping the flow rate constant over 20 experimental points, for 1 minute each, in the volumetric flow rate range [0.6-1.3] [l/s].

The error treatment was carried out considering a confidence interval of 95%. Figure 3 shows the relative error of FT-W_C1, FT-W_C2 and calibrator sensors as a function of volumetric flow rate. The relative error turns out to be higher for sensor FT-W_C2 than for sensor FT-W_C1. The two sensors share the same operating principle but are made of different materials and have different type of insertion into the flow. For this reason, sensor FT-W_C2 has about twice the error of sensor FT-W_C1.

Since they measure the same physical quantity, it is possible to use the Data Reconciliation (DR) technique to reduce the relative error to even less than that of the most accurate sensor (FT-W_C1). This technique also makes it possible to assess whether or not gross errors are present, through Gross Error Detection (GED). In particular, DR can only be carried out if the experimental measurement is not affected by gross error, but only by random error. The technique adopted in this paper to perform DR is that of Lagrange multipliers, as recommended by [20].
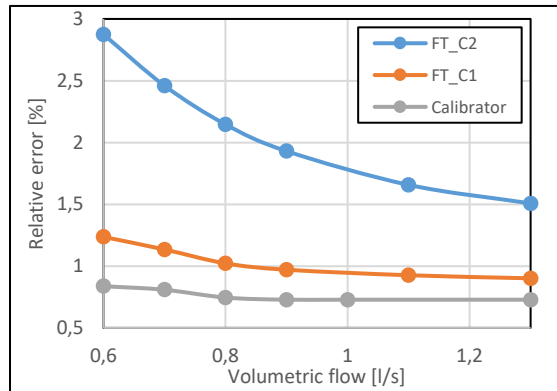

Figure 3 – FT-W_C1, FT-W_C2 and Calibrator relative errors as a function of volumetric flow rate

The goal of data reconciliation is to minimize the difference between the measurements (y) and the reconciled data (x), using the uncertainties of the measurements as weights. This can be written as:

$$MIN_{(x,u)}(y - x)^T \Sigma^{-1}(y - x) \qquad (1)$$

Such an optimization problem must be subject to constraints, expressed according to equations (2) and (3):

$$f(x,u) = Ax = 0 \qquad (2)$$

$$g(x,u) \leq 0 \qquad (3)$$

where:

Σ: Variance-covariance matrix.

x: Vector of reconciled variables.

y: Vector of measured values of variables x.

u: Vector of unmeasured variables.

f: Vector of equality constraints (balance equations)

g: Vector of inequality constraints

A: Constraint matrix.

The Σ matrix contains variances (on the diagonal) and covariances of measurement accuracy and their correlation.

'A' is a matrix of dimension [m x n]. The m rows correspond to the constraints. It can be easily verified that for a flow reconciliation problem, the elements of each row of matrix A are either +1, -1 or 0, depending on whether the corresponding stream flow is input, output or, respectively, not associated with the process unit for which the flow balance is written. This approach is based on the fact that any mass or energy conservation law can be expressed in the following general form:

$$In + Gen - Out - Con - Acc = 0 \qquad (4)$$

where:

In = Input

Gen = Generation

Out = Output

Con = Consumption

Acc = Accumulation

In case of linear systems, the analytical solution to the above problem can be obtained using the method of Lagrange multipliers:

$$\hat{x} = y - \Sigma^{-1}A^T(A\Sigma^{-1}A^T)^{-1}Ay$$
$$= y - v \qquad (5)$$

Where v is the vector of improvements (measurement adjustments). The application case of FT-W_C1 and FT-W_C2 flow rates is extremely simple and is based on the balance equation (6):

$$\dot{V}_{FT_{C1}} - \dot{V}_{FT_{C2}} = 0 \qquad (6)$$

Hence:

$$y = [\dot{V}_{FT_{C1}} \ \dot{V}_{FT_{C2}}]^T \qquad (7)$$

$$\Sigma = \begin{bmatrix} \sigma_{FT_{C1}}^2 & 0 \\ 0 & \sigma_{FT_{C1}}^2 \end{bmatrix} \qquad (8)$$

$$A = [1 \ -1] \qquad (9)$$

For a more in-depth explanation of the method, the publication [20] is referred. The resolution of Lagrange's method provides a new value for the volumetric flow rate, with a lower uncertainty than the more accurate of the two sensors.

A similar procedure is carried out on condenser-side temperature measurements, where a DIN1/10 resistance thermometer and a T-type thermocouple are in series. In the temperature range [0-60] [°C] that is encountered in this activity, the error given by the sensor and measurement chain is 0.18°C for the DIN1/10 RTD and 0.90°C for the T-type TC (95% confidence interval). Because the error difference between the two sensors is larger, the error is reduced less with the DR technique.

The authors have decided to install this type of sensors to combine good accuracy (guaranteed by RTD) with a good dynamic response (thermocouple).

2.3 Refrigerant mass flow calculation

In the test rig, there is no flow meter inside the chiller loop. The energy balance at the condenser is then used to indirectly calculate the flow rate. Referring to Figure 1 the law of conservation of energy applied to the condenser returns eq. (10) (thermal losses are considered negligible, this assumption being a potential source of error):

$$\dot{m}_W \cdot (h_{W-C2} - h_{W-C1}) = \dot{m}_R \cdot (h_{R-C1} - h_{R-C2}) \qquad (10)$$

It then turns out that it is possible to calculate the refrigerant flow rate $\dot{m}_R$ as reported in (11):

$$\dot{m}_R = \frac{\dot{m}_W \cdot (h_{W-C2} - h_{W-C1})}{(h_{R-C1} - h_{R-C2})} \qquad (11)$$

What is clear from this equation is that, in order to obtain a true-to-reality result, it is necessary to have excellent accuracy in the calculation of water flow rate and in the calculation of temperatures and pressures. Once the refrigerant flow rate is known, the reduced refrigerant flow rate can be calculated, using those at the compressor inlet (that is, at the evaporator outlet) as thermodynamic parameters:

$$\dot{m}_{R-red} = \frac{\dot{m}_R \cdot \sqrt{\dfrac{T_{T-E2}}{T_{Ref}}}}{\dfrac{P_{T-E2}}{P_{Ref}}} \qquad (12)$$

where:

$T_{Ref} = 15°C = 288.15K$

$P_{Ref} = 1\ bar = 10^5 Pa$.

The experimental error on the reduced refrigerant flow rate is then expressed by (13) which was obtained from the error propagation laws.

$$\frac{\Delta \dot{m}_{R-Red}}{\dot{m}_{R-Red}} = A + B + C + D + E \qquad (13)$$

where:

$$A = \frac{\Delta \dot{m}_W}{\dot{m}_W} \qquad (14)$$

$$B = \frac{\Delta h_{W-C2} + \Delta h_{W-C1}}{|h_{W-C2} - h_{W-C1}|} \qquad (15)$$

$$C = \frac{\Delta h_{R-C1} + \Delta h_{R-C2}}{|h_{R-C1} - h_{R-C2}|} \qquad (16)$$

$$D = \frac{\Delta T_{T-E2}}{2 \cdot T_{T-E2}} \qquad (17)$$

$$E = \frac{\Delta P_{T-E2}}{P_{T-E2}} \qquad (18)$$

The following is a brief description of each contribution:

A) Error on the flow rate of cooling water to the condenser. This relative error is visible in Figure 3.

B) Error on the enthalpies of water. Since water is incompressible, the error on the enthalpies of water is only a function of the error in the temperature measurement.

C) Error on the enthalpies of refrigerant. In this case, the error is a function of both the error in the pressure measurement and the error in the temperature measurement.

D) Error on the total temperature at the compressor inlet. Because the compressor inlet speeds are very low, the error on the dynamic component is assumed to be negligible. Overall error is therefore given by the sensor and the temperature measurement chain.

E) Error on the total pressure at the compressor inlet. Because the compressor inlet speeds are very low, the error on the dynamic component is assumed to be negligible. Overall error is therefore given by the sensor and the pressure measurement chain.

3. RESULTS AND DISCUSSION

For the analysis of the compressor performance the following sensor set-up will be used, to evaluate and compare the results obtained with different kind of sensors:

- *Set-up n.1* = is the least performing set up and is composed by the thermocouple on water side circuit (TC-W_E1/2; TC-W_C1/2) and FT-C2 as water mass flow sensor.

- *Set-up n.2* = is the best performing set up and is composed by the RTD on water side circuit

(RTD-W_E1/2; RTD-W_C1/2) and FT-C1 as water mass flow sensor

All measurements done on refrigerant side are the same for each future analysis, since there are no redundant sensors installed.

3.1 Compressor map

Regarding the high-speed radial compressor installed in the prototype heat pump loop, different operating curves at different reduced speeds were obtained thanks to a dedicated characterization campaign.

Keeping the same reduced speed, defined in (19), the operative conditions of the compressor were modified by changing the evaporator and compressor temperatures - thus, changing their pressures and the compressor total-to-static pressure ratio β, defined in (20).

The system reacts to these changes finding a new operative condition characterized by a different reduced mass flow, which was measured as described in Par 2.3.

$$n_{red} = \frac{n}{\sqrt{\dfrac{T_{T-E2}}{T_{Ref}}}} \qquad (\ 19\ )$$

$$\beta_{red} = \frac{P_{C1}}{P_{T,E2}} \qquad (\ 20\ )$$

Each curve is composed by almost five operative points, and each of these points was obtained running the system for 30 minutes while maintaining constant conditions, so that thermal regime is ensured.

The number of operative points evaluated is 26 (6 points for 70% speed curve, and 5 points for the others).

Figure 4 shows the compressor chart, where five curves at different reduced speed are represented: 70%, 81%, 87%, 92% and 98% of the reduced speed, calculated as a function of the shaft speed through eq. (19). The maximum shaft speed corresponds to 75000 rpm.
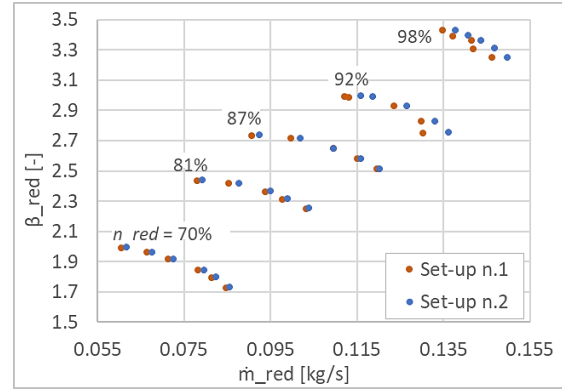

Figure 4 – Compressor characteristic map

As clearly visible from Figure 4, these iso-speed curves (identified by the red and blue points) are quite the same for low speeds, but at high speed (and therefore close to the nominal speed of the compressor itself) the distance between blue and red dots increases, highlighting significant differences, especially on the value of the reduced flow rate. In particular, the reduced mass flow evaluated according to the measurement done with the Set-up n.1 are lower than the ones evaluated with Set-up n.2.

For this reason, Data reconciliation techniques were applied, as mentioned in Section 2.2, to increase the accuracy of the process parameters evaluated. These techniques were applied to all the operative points, but here focus is on the 92% and 98% reduced speed curves. In fact, these are the curves characterized by the highest discrepancies.

Figure 5 shows the operative points obtained with Set-up n.1 (red dots), the ones obtained with the Set-up n.2 (blue dots) and, finally, the green crosses indicate the operative points obtained after the application of data-reconciliation.
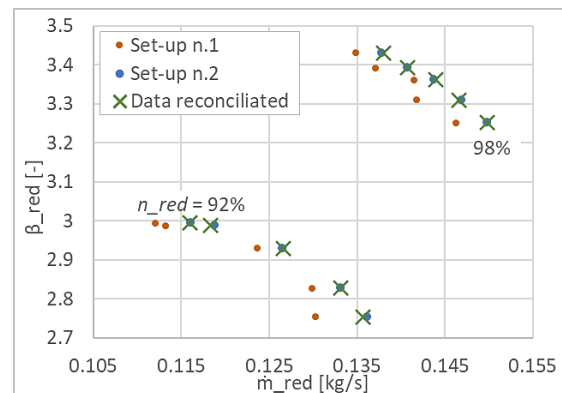

Figure 5 – Compressor iso-speed 92% and 98% curves obtained with Set up 1, Set up 2 and with Data Reconciliation techniques

As expected, the reconciled operating points are close to the ones obtained with the direct measurement done with Set-up n.2, which is the most accurate. In fact, as already explained in

Section 2.2, the different measures are merged through a specific weightage proportional to the accuracy of the different measurements themself.

3.2 Relative error on refrigerant mass flow

The analysis of the relative error focuses on the most critical parameter evaluated during the experimental campaign, i.e., the refrigerant reduced mass flow inside the heat pump loop. This is indirectly calculated through the energy balance at the condenser on all 26 operating points previously introduced.

Hereafter, the focus is on the results obtained on the operating points characterized by the lowest precision (Test n.6) and the one characterized by the best precision (Test n.12).

Test n. 6 refers to the incipient surge conditions at the reduced rotational speed of 70%, which is the last point of complete stability before encountering the surge (near-surge). The heat power at the condenser is, under these conditions, the lowest in the entire compressor map. For this reason, this point turns out to have the largest relative error.

Test No. 12 is the most far from the surge in the reduced speed curve of 87%.

Table 3 shows the main averaged process parameters measured during these tests.

Parameter	Test n.6	Test n.12
FT-W_C1 [l/s]	0.68	0.70
FT-W_C2 [l/s]	0.69	0.71
TC-W_C1 [°C]	32.9	31.2
TC-W_C2 [°C]	37.6	40.0
RTD-W_C1 [°C]	33.3	31.7
RTD-W_C2 [°C]	38.1	40.6
RTD-R_C1 [°C]	49.0	60.6
RTD-R_C2 [°C]	40.2	44.9
RTD-R_E2 [°C]	25.8	24.1
PT-R_C1 [bar(a)]	2.37	2.87
PT-R_C2 [bar(a)]	2.37	2.85
PT-R_E2 [bar(a)]	1.19	1.14

Table 3 – Direct measurements in Test n.6 and Test n.12

Figure 6 shows the relative error obtained through the experimental Set-up n.1, Set-up n.2 and reconciliated data, for both Test n.6 and Test n.12.
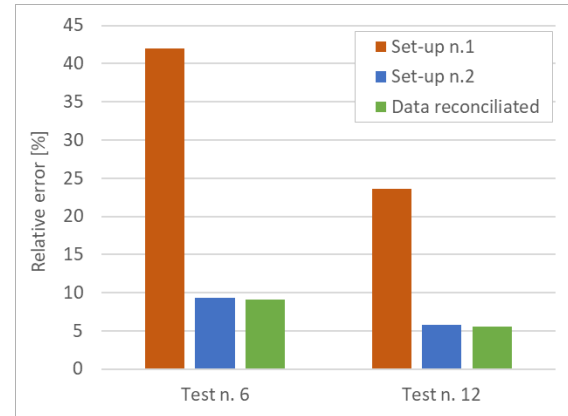

Figure 6 – Relative error comparison between Test n.6 and Test n.12

The relative error obtained thanks to Set-up n.1 exceeds 40% in Test n.6 and reaches 25% in Test n.12. This makes Set-up n.1 unreliable for the evaluation of the refrigerant reduced mass flow. On the other hand, Set-up n.2 allows obtaining relative errors below 10% in Test n.6 and close to 6% in Test n.12. Figure 6 also shows the relative error obtained through the application of the data reconciliation techniques for both tests. The reduction of the relative error is evident, despite not significant. In fact, the final value of the relative error is obtained through a weighted balance of the different measure chains: in this case, the first set-up has a relative error significantly higher than the second one.

As explained in Section 2.3, the relative error of the refrigerant reduced mass flow is evaluated in accordance with the error propagation theory, and is composed by five contributions:

A) Error on the flow rate of cooling water to the condenser

B) Error on the enthalpies of water.

C) Error on the enthalpies of refrigerant.

D) Error on the total temperature at the compressor inlet.

E) Error on the total pressure at the compressor inlet.

Figure 7 allows to compare these different contributions for Set-up n.1, Set-up n.2 and reconciliated data for both Test n.6 and Test n.12.

Contributions (D) and (E) together represent around 0.5% of the global relative error, in both Test n.6 and n.12 and considering different Set-ups. These contributions are, in fact, associated with the inlet temperature and inlet pressure, and as per eq. (12), are used to calculate the reduced mass flow. It can be noted that, since in this formula the temperature is inside a squared root, the associated relative error in the contribution (D) is divided by 2.
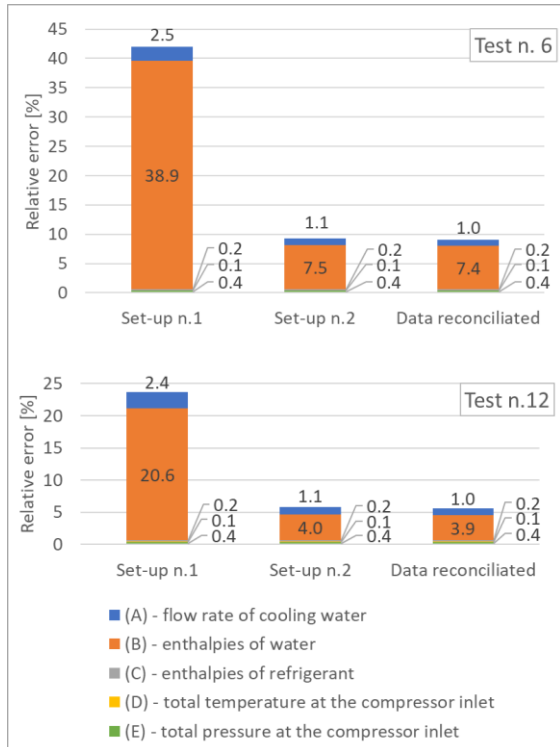
Figure 7 – Relative error contributions in Test n.6 and Test n.12

Contribution (C) is also not that relevant, as this error is associated with the relative error calculated in the evaluation of the enthalpy difference between the inlet and outlet of the condenser. Since there is a phase change in the refrigerant in this component, the enthalpy difference is very high, and the relative error of this parameter is consequently low.

Looking at the contributions (A) and (B), which are the main relative error sources, it can be noted that:

- Contribution (A) is quite the same for both Test n.6 and Test n.12. This is due to maintaining an approximately constant water flow rate under the two operating conditions.
- Applying data reconciliation techniques allows to reduce this contribution, compared to the Set-up n.2, of about 10% in Test n.6 and Test n.12 (from 1.1% to 1%)
- The main difference between Test n.6 and Test n.12 in terms of relative error is caused by contribution (B). Applying data reconciliation techniques do not allow to significantly reduce this contribution, which in both cases is reduced only by about 2%.

The difference between the relative errors associated with the contribution (B) for Set-up n.1 and Set-up n.2 is consistent. It can be noted that the relative error of contribution (B) for Set-up n.1 is around five times the one of the Set-up n.2, in both Test n.6 and Test n. 12.

The effectiveness of the application of data reconciliation techniques in the case of contribution (A) is guaranteed by the fact that these measurements are affected by a relative error similar for both Set-up n.1 and Set-up n.2. In fact, this contribution is connected only to the relative error of the mass flow sensors, which are the same models and installed in different pipes, as previously described.

In the Set-up n.2, the contribution (B) represents around 70-80% of the overall relative error, in both Test n.6 and Test n.12.

This can be explained owing to the fact that the temperature difference at the condenser – water side – is low. In Test n.6 the temperature difference between the condenser inlet and outlet is around 5°C, while in Test n.12 is around 9°C. As shown in Par. 2.1, the thermocouples have an error of 0.9 °C, while RTDs have an error of 0.18 °C.

All these elements make the influence of the data reconciliation techniques ineffective and not that useful for this case. In both tests, the reduction in error that is achieved with date reconciliation compared with Set-up n.2 is about 3%. More precisely, the error on reduced refrigerant flow rate goes from 9.3% to 9% in Test n.6 and from 5.8% to 5.6% in Test n.12.

Since the main contribution is directly related to the temperature difference between condenser inlet and outlet on water side, and this temperature difference depends on the mass flow, a sensitivity analysis to evaluate impact of the water flow variation on the effectiveness of the data reconciliation techniques is carried out in the following.

3.3 Sensitivity analysis

In order to evaluate the impact of the mass flow of the water at the condenser, which influences the relative error of both the contributions (A) and (B), the Test n.6 has been chosen as reference. Assuming the same working condition of the heat pump (and the same thermal power released at the condenser) different mass flows and consequently different temperature difference at the condenser were imposed. Sensitivity analysis was carried out up to a flow rate value of 0.2 l/s by extrapolating the relative error curves of the flow sensors up to this value. In addition, the same analysis was performed assuming two DIN 1/10 RTDs instead of the paired DIN 1/10 RTD – TC Type T. The analysis was not carried out on the less precise Set-up n.1 in order to highlight the achievable improvements over the more effective Set-up n.2. Figure 8 shows the relative error on the refrigerant reduced mass flow as the flow rate of water to the condenser changes.
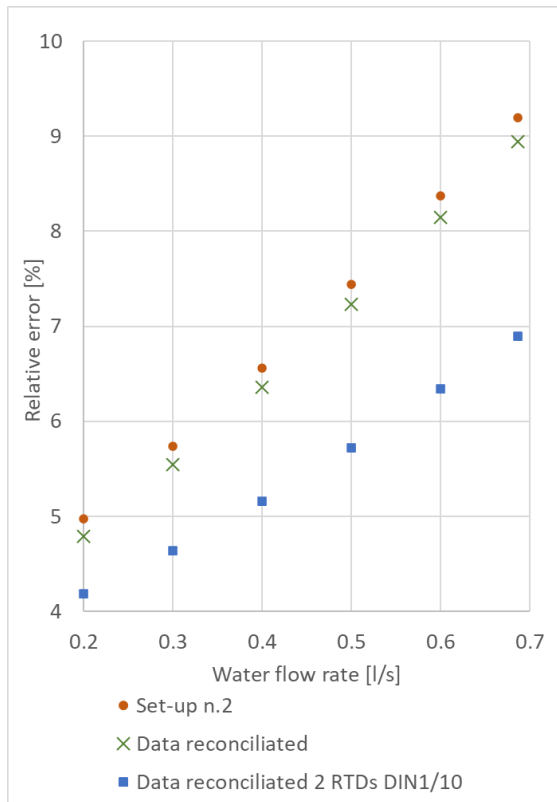
Figure 8 – Relative error as a function of water flow rate to condenser, Test n.6.

The graph shows how the error can be reduced by reducing the water flow rate to the condenser. The error curve for flow rate less than 0.6l/s is not known, as visible in Figure 3. If extrapolation is considered consistently, the increase in error on water flow rate turns out to be less than the decrease in error related to the higher temperature difference between condenser inlet and outlet. With a flow rate of 0.2 l/s, the relative error achievable with the data reconciliation would seem to fall slightly below 5 percent. At the same flow rate, if two DIN1/10 RTDs were used, the error would be about 4.2%. Therefore, to obtain the reduced refrigerant flow rate with good accuracy through the energy equation, it is necessary to use low water flow rates to the condenser and very accurate temperature sensors.

4. CONCLUSIONS

The studies conducted in this test rig shows the effective application of data reconciliation and sensitivity analysis for performance evaluation of dynamic compressors in a closed loop, 2-phase circuit for innovative heat pumps. The performance of the compressor has been studied through dedicated experimental campaign, and the compressor characteristics map has been developed, with the help of data reconciliation techniques, to increase the accuracy of measurements. Analysis of the relative error on the refrigerant mass flow rate is also performed to ensure the fidelity of indirect mass flow calculations, and the contribution of different parameters are determined. The sensitivity analysis conducted on mass flow rate measurement shows that the error can be reduced significantly by using lower water flow rates to condenser and accurate temperature sensors.

In particular, this study raised that an average reduction of 4% on the relative error is achievable by reducing the mass flow by 3.5 times while, by keeping the same mass flow and using only RTD DIN 1/10, the reduction of the relative error is between 0.8 and 2%, depending on the mass flow itself. This led to conclude that both actions are helpful to increase the accuracy of the data acquisition system. However, varying the mass flow rate could affect the correct operations of the HP itself, so, this parameter should be chosen carefully.

This study is a leap forward towards the optimized use of instrumentation and analysis techniques on heat pumps, while simultaneously maintaining a higher level of accuracy. And, in the coming years, such methods would significantly improve the condition monitoring of the heat pump systems.

REFERENCES

[1]   P. Baggio, E. Bee, and A. Prada, "Demand-side management of air-source heat pump and photovoltaic systems for heating applications in the italian context," *Environments - MDPI*, vol. 5, no. 12, 2018, doi: 10.3390/environments5120132.

[2]   A. Rinaldi, M. C. Soini, K. Streicher, M. K. Patel, and D. Parra, "Decarbonising heat with optimal PV and storage investments: A detailed sector coupling modelling framework with flexible heat pump operation," *Applied Energy*, vol. 282, p. 116110, Jan. 2021, doi: 10.1016/J.APENERGY.2020.116110.

[3]   K. J. Chua, S. K. Chou, and W. M. Yang, "Advances in heat pump systems: A review," *Applied Energy*, vol. 87, no. 12. 2010. doi: 10.1016/j.apenergy.2010.06.014.

[4]   Reboli Tommaso *et al.*, "Gas Turbine Combined Cycle Range Enhancer - Part 1: Cyber-physical setup," *Proceedings of ASME Turbo Expo*, 2022.

[5]   M. Ferrando, A. Renuke, A. Traverso, and V. Sishtla, "A new design method for two-phase nozzles in high efficiency heat pumps," *International Journal of*

Refrigeration, vol. 127, pp. 148–156, 2021.

[6] "Carrier introduces turbine technology," *Refrigeration and air conditioning*, pp. 31–32, 1994.

[7] J. Song, J. C. Park, K. Y. Kim, J. Jeong, and S. J. Song, "Surge onset in turbo heat pumps," *Journal of Turbomachinery*, vol. 136, no. 8, 2014, doi: 10.1115/1.4026145.

[8] S. Marelli, A. Misley, and M. Ferrando, "Experimental investigation in turbocharger compressors during surge operation," *Proceedings of ASME Turbo Expo*, Jun. 2020.

[9] M. L. Ferrari, P. Silvestri, F. Reggio, and F. A. Massardo, "Surge prevention for gas turbines connected with large volume size: Experimental demonstration with a microturbine," *Applied Energy*, vol. 230, pp. 1057–1064, 2018.

[10] M. L. Ferrari, P. Silvestri, M. Pascenti, F. Reggio, and A. F. Massardo, "Experimental dynamic analysis on a T100 microturbine connected with different volume sizes," *Journal of Engineering for Gas Turbines and Power*, vol. 140 (2), 2018.

[11] H. R. Kim and S. J. Song, "Modeling of surge characteristics in turbo heat pumps," in *Proceedings of the ASME Turbo Expo*, 2010, vol. 7, no. PARTS A, B, AND C. doi: 10.1115/GT2010-23342.

[12] E. M. Greitzer and F. K. Moore, "A theory of post-stall transients in axial compression systems: Part II—application," *Journal of Engineering for Gas Turbines and Power*, vol. 108, no. 2, 1986, doi: 10.1115/1.3239893.

[13] F. K. Moore and E. M. Greitzer, "A theory of post-stall transients in axial compression systems: Part 1—development of equations," *Journal of Engineering for Gas Turbines and Power*, vol. 108, no. 1, 1986, doi: 10.1115/1.3239887.

[14] B. W. Botha, B. du Toit, and P. G. Rousseau, "Development of a mathematical compressor model to predict surge in a closed loop Brayton cycle," in *American Society of Mechanical Engineers, International Gas Turbine Institute, Turbo Expo (Publication) IGTI*, 2003, vol. 3. doi: 10.1115/GT2003-38795.

[15] "Model 206 | Industrial Pressure Sensor." https://www.setra.com/products/pressur e/model-206-industrial-pressure-transducer?hsLang=en (accessed Aug. 03, 2022).

[16] "TEMPERATURE MONITORING." Accessed: Aug. 03, 2022. [Online]. Available: https://media.trafag.com/literature/catal ogue/H76003_EN_Products_catalogue _Temperature_monitoring_hires.pdf

[17] "PADDLEWHEEL FLOW SENSOR SAFETY INSTRUCTIONS", Accessed: Aug. 03, 2022. [Online]. Available: http://www.flsnet.it/download/20160801 104030_I2366-IMF300E-REV-02.pdf

[18] M. E. Mondejár, M. O. McLinden, and E. W. Lemmon, "Thermodynamic Properties of trans-1-Chloro-3,3,3-trifluoropropene (R1233zd(E)): Vapor Pressure, (p, ρ, T) Behavior, and Speed of Sound Measurements, and Equation of State," *J. Chem. Eng. Data*, vol. 60, pp. 2477–2489, 2015.

[19] "Proline Prosonic Flow 91W Ultrasonic flowmeter | Endress+Hauser." https://www.endress.com/en/field-instruments-overview/flow-measurement-product-overview/ultrasonic-flowmeter-prosonic-flow-91w?t.tabId=product-overview (accessed Mar. 10, 2022).

[20] "Verein Deutscher Ingenieure 2048, Uncertainties of measuerement during acceptance tests on energy-conversion and power plants fundamentals," Oct. 2000.

10